The CoREST-complex regulates MYC stability and promotes post-transcriptional mRNA splicing in melanoma

Abdul A Khan[1], Ariel A Aptekmann[1], Jaemin Byun[1], Dongkook Min[1,4], Michael C Povelaitis[1], JiYeon Shin[1,2], Johannes L Zakrzewski[1,2,3,] and Byungwoo Ryu[1,2]

[1]Center for Discovery and Innovation, Hackensack Meridian Health, Nutley, NJ 07110, USA.

[2]Department of Oncology, Georgetown University, Washington DC, 20057, USA.

[3]Department of Pediatrics, Hackensack University Medical Center, Hackensack, NJ 07601, USA.

[4]Current address: Krantz Family Center for Cancer Research, Massachusetts General Hospital Cancer Center, Charlestown, MA 02129, USA.

Running Title: The CoREST complex stabilizes MYC and promotes RNA processing.

Corresponding Author:

Byungwoo Ryu, Center for Discovery and Innovation, Hackensack Meridian Health, 111 Ideation Way, Nutley, NJ 07110.

Email: byungwoo.ryu@hmh-cdi.org

Conflict of Interest:

The authors declare that they have no conflict of interest regarding this manuscript.

Word count: 5556

Figures and Tables:

4 main Figures

3 Supplementary Figures

2 Supplementary Tables

Abstract

The maturation of RNA is mediated by the coordinated actions of RNA-binding proteins through post-transcriptional pre-mRNA processing. This process is a central regulatory mechanism for gene expression and plays a crucial role in the development of complex biological systems. MYC directly upregulates transcription of genes encoding the core components of pre-mRNA splicing machinery. The perturbation of splicing processes is associated with various disease conditions, including cancer. Here, we report that the CoREST complex stabilizes MYC from proteolytic degradation via post-translational modification through site-specific deacetylation of lysine residues. Furthermore, the CoREST complex acts as a transcriptional coregulator of MYC-driven transcriptional activation of RNA processing genes. These genes include those encoding snRNPs and snoRNPs that are important players in pre-mRNA spliceosome fidelity. Genetic ablation and pharmacological inhibition of the CoREST complex in melanoma cells induce altered spliceosome activity. These alterations result in significant changes in genome-wide expression patterns of alternatively spliced mRNA isoforms and compromise cell survival. The ectopic expression of one of the RNA processing genes, NOLC1, partially restores cell viability in the CoREST complex-depleted cells. These findings identify the interaction of the CoREST-complex with MYC as a central regulator of cancer-specific expression profiles of mRNA splicing variants.

Significance

The pathogenic role of the CoREST complex in cancer is not well-defined. Our study reveals that the CoREST complex stabilizes MYC protein in melanoma cells and acts as a coregulator for activating RNA processing genes. Disrupting the CoREST-MYC axis alters genome-wide alternative splicing patterns, suggesting a potential therapeutic target for MYC-driven cancers, including melanoma.

Introduction

CoREST/RCOR1 (REST co-repressor 1) was initially identified as a co-repressor of REST/NRSF (RE1 Silencing Transcription factor/Neural-Restrictive Silencer Factor), a DNA binding transcription factor that recruits CoREST to repress neuronal-specific gene transcription in non-neuronal cells for developmental processes (1). CoREST forms a multi-subunit transcriptional co-regulator complex by recruiting two histone-modifying enzymes: Class I histone deacetylase 1 or 2 (HDAC1/2) (2) and lysine-specific histone demethylase 1A (LSD1/KDM1A) (3). The RCOR1-HDAC1/2-LSD1 complex (CoREST-complex) is considered a transcriptional repressor by erasing active histone modifications, such as histone acetylation and mono- and di-methylations of histone H3 lysine 4 (H3K4me1/2) (1-4). Transcription factors such as REST, Gfi-1/Gfi-1b, and Nurr1 are known as recruiters of the CoREST-complex to nucleosomes for regulation of their target gene transcription (1,5,6). Structural evidence of the CoREST-complex suggested that it also interacts with chromatin without bona fide transcription factors, as its binding affinity to either naked or nucleosomal DNA varied with monovalent ion concentrations and inter-nucleosomal DNA lengths (7,8). These experimental results suggested that electrostatic interactions and accessible nucleosome conformations are also critical factors governing the direct binding of the complex to chromatin for transcriptional regulation (8,9).

In a recent study of genome-wide bindings of the complex in mammalian cells, the CoREST-complex was found to preferentially bind to proximal promoters of highly expressed genes at transcriptionally permissive chromatin loci in euchromatin and act as a transcription rheostat (10). Interestingly, studies have also shown that the CoREST-complex interacts with transcription co-factors, such as hormone (androgen and estrogen) receptors and NeuroD1 transcription factor, and is able to promote their target gene transcription (11-13), suggesting an additional role for post-translational modifications (PTMs) of non-histone proteins such as transcriptional cofactors in transcriptional activation.

MYC overexpression is found in over 50% of human cancers and is associated with poor prognosis and aggressive tumor behavior (14,15). MYC protein is tightly controlled in normal cells, with a half-life of about 20 minutes, via post-translational modifications (PTMs)-linked rapid protein degradation, mediated by the ubiquitin-proteasome system (16,17). This cellular MYC homeostasis is dysregulated in cancer cells, where overexpressed MYC promotes malignant progression and tumor maintenance (14,18). The effects of MYC acetylation on its stability are multifaceted and context-dependent. While acetylation by acetyltransferases like p300/CBP and GCN5/PCAF generally increases MYC stability by inhibiting ubiquitination (19,20), p300-mediated MYC acetylation has also been linked to its increased proteasomal degradation (20,21). Similarly, HDACs, such as SIRT1 and HDAC1/2-containing SIN3 complex, have been reported to deacetylate MYC and either stabilize or destabilize MYC depending on cell type and cellular context (22,23). The functional outcome of MYC acetylation can also vary based on specific acetylation/deacetylation sites and cellular context (24).

Here, we report a distinctive role of the CoREST-complex in regulating post-transcriptional RNA processing in cancer cells by increasing oncoprotein MYC stability via site-specific post-translational deacetylation of MYC lysine residues.

Results

The CoREST-complex physically interacts with and stabilizes MYC from proteolytic degradation in melanoma cells.

Since *MYC* gene amplification in melanoma patients is associated with metastasis and therapy resistance (25) and the deacetylases (SIRT1 and SIN3 complex) regulate MYC stability (22,23,26), we intended to test the possibility of MYC regulation by the CoREST-complex in cancer cells. First, to address whether MYC and CoREST-complex are in close proximity in cells, we performed proximity ligation assays (PLAs) between MYC and each core component of the CoREST-complex (HDAC1/2, RCOR1, and LSD1), and confirmed that MYC and each

member of the CoREST-complex were located exclusively in cell nuclei in close proximity (Fig. 1A). This observation supports the possibility of physical interaction between the CoREST-complex and MYC. We also verified the direct MYC interaction *in vitro* and in cells with the CoREST-complex by co-immunoprecipitation (co-IP) assay. Recombinant histidine (his)-tagged full-length MYC was incubated with MeWo and WM983B melanoma cell lysates, and co-IPs of RCOR1 by MYC, and reciprocally co-IPs of MYC by RCOR1 confirmed the binding (Fig. 1B). The same co-IP assays in cells (HEK293T) expressing FLAG-tagged MYC and HA-tagged RCOR1, respectively, were performed and recapitulated the protein-protein interaction observed in the *in vitro* assays (Fig. 1B). MYC was also co-IPed by LSD1 in both *in vitro* and in cell experiments, again suggesting that the core CoREST-complex is the entity interacting with MYC.

Although it is unclear which core component of the CoREST-complex directly interacts with MYC, our studies mapping the interaction domain in MYC for the CoREST-complex using the FLAG-tagged MYC domain deletion mutants suggested that the DNA binding C-terminal region harboring a basic-helix-loop-helix leucine zipper (b-HLH-LZ) domain is essential for interaction with the CoREST-complex since all the mutants without the C-terminal region showed no or limited binding affinity (Supplementary Fig. S1). Previous studies by others showed that MYC binding domain III (MBIII) interacts with histone-modifying complexes, such as HDAC3 and SIN3 (27,28) ; however, the N- and C-terminal truncated central region only containing the MBIIIb and MBIV domains had no binding affinity with RCOR1. On the other hand, the full-length MYC, with both MBIIIb and MBIV domain deletion or each deletion of MBIIIb domain and MBIV domain showed no changes in binding affinity compared to the full-length wildtype MYC (Supplementary Fig. S1B). Altogether, this deletion mutant analysis strongly suggests that the C-terminal, which is known to be essential to hetero-dimerize with a transcriptional factor MAX (MYC associated Factor X) for DNA binding, is an essential domain for interaction with the CoREST-complex.

We also observed that the CoREST-complex stabilized MYC protein from proteolytic degradation in melanoma cells. RCOR1 knockdown (KD) caused a decrease in the MYC protein level which was reversed by proteasome inhibitor MG132 treatment (Fig. 1C). Yet, ectopic overexpression of hemagglutinin-tagged RCOR1 (HA-RCOR1) in melanoma cells (WM983B and SK-MEL2) induced a significantly increased MYC level (Fig. 1D), suggesting that MYC post-translational modifications (PTM) mediated degradation either by the HDAC1/2 or LSD1 within the CoREST-complex is a major regulatory mechanism of MYC homeostasis in melanoma cells. This notion was supported by the positive correlations between the expression levels of MYC and RCOR1 in a panel of fourteen melanoma cell lines (Fig. 1E). Moreover, there were no significant changes in MYC transcript levels by the RCOR KD compared to control cells (Fig. 1G) while the expression of known MYC target genes (*CCNA2, Mad2L1, MCM4, RRM1,* and *TYMS*) was significantly decreased (Fig. 1F). We also observed that depletion of each member of the CoREST-complex, RCOR1 and LSD1, induced an increased apoptotic cell fraction, leading to growth inhibition in multiple melanoma cell lines. This phenotype was recapitulated by MYC depletion (Fig. 1H), suggesting that to some extent the CoREST-complex may exert oncogenic effects via increased levels of MYC protein.

HDAC1/2 in the CoREST-complex regulates MYC stability via site-specific lysine deacetylation.

To determine which enzyme in the CoREST-complex (HDAC1/2 or KDM1A) plays a role in the PTM-mediated MYC stabilization, we treated WM983B cells with MS275 (Entinostat), a class I HDAC inhibitor (HDACi), LSD1 inhibitor (LSD1i) GSK2879552, MS275 + GSK2879552 combination (HDACi + LSD1i), and a dual-action inhibitor of HDAC1/2 and LSD1, Corin (29), and found that Corin was the most effective in decreasing MYC protein level. The histone demethylase inhibitor (LSD1i) showed no effect (Fig. 2A). Genetic knockdown (KD) of HDAC2 showed decreased MYC protein level in WM983B cells while no changes were observed by

HDAC1 depletion (Supplementary Fig. S2A), suggesting that HDAC2 in the CoREST-complex contributes to the proteolytic regulation of MYC. Pharmacologic inhibition of the CoREST-complex by Corin induced decreased MYC levels in a panel of 10 melanoma cell lines, further supporting MYC stabilization by the CoREST-complex via protection from PTM-mediated proteolytic degradation (Supplementary Fig. S2B). Furthermore, decreased MYC levels by CoREST-complex inhibitors (Fig. 2A) closely matched the growth inhibition patterns in melanoma cell lines (SK-MEL2 and 1205Lu) (Supplementary Fig. S2C).

To find the potential lysine residues targeted by CoREST-complex, we performed site-directed mutagenesis by ectopically expressing mutant forms of MYC with specific lysine-arginine substitutions. First, we identified 11 predicted post-translational lysine acetylation residues in MYC using the online tool GPS-PAIL (30). Next, we treated the cells with Corin and quantified the mutant MYC levels by immunoblots followed by ImageJ analyses. The quantification of each mutant MYC protein level suggested five lysine residues as potential deacetylation target sites (K148, K157, K275, K289, and K323) of the CoREST-complex (Fig. 2C). The mutant form of MYC in which all five lysine residues were substituted by arginine (MYC-DR) was ectopically expressed in the melanoma cells. The protein level of MYC-DR was higher than that of the wild-type MYC (MYC-WT) in RCOR1-KD and control cells, and MYC-DR was also resistant to proteolytic degradation in the RCOR1-KD cells compared to the control cells (Fig. 2D). A similar trend was also observed in cells (WM983B and A375) where the enzymatic activity of HDAC2 in the CoREST-complex was inhibited by Corin treatment (Fig. 2E).

These experimental data strongly suggest that deacetylation of MYC at these lysine residues by the CoREST-complex stabilizes MYC from proteolytic degradation in melanoma by counterbalancing the acetylation of the lysine residues mediated by lysine acetyltransferases (KATs). This notion was supported by the significantly decreased MYC levels in lenti-X-293T cells stably overexpressing p300 and CBP (Fig. 2F). P300 protein has been observed to regulate the expression of MYC transcriptionally as well as at the post-translational level (20).

To avoid the transcriptional regulation of MYC gene expression by p300/CBP, we used stably expressing HA-tagged MYC in melanoma cells (WM983B) and treated with a selective p300/CBP HAT inhibitor (HATi) A485 (31). The A485 treatment recovered the MYC protein level which was reduced by Corin treatment (Fig. 2G). Furthermore, increased ubiquitination in MYC-WT compared to MYC-DR by Corin treatment (Fig. 2H) and increased stability of MYC-DR compared to MYC-WT in the cells treated with cycloheximide (Fig. 2I) strongly indicate that the site-specific deacetylation of MYC by HDAC2 in the CoREST-complex stabilizes MYC from proteolytic degradation in melanoma.

To assess the pathologic roles of increased MYC protein stability in melanoma, overall survival of melanoma patients with high and low expression of MYC protein and transcript levels, respectively, was determined by analysis of cumulative survival probabilities (Kaplan-Meier curves). Patient stratification based on MYC protein levels showed a significant inverse association with survival, while no association was found with MYC transcription levels, suggesting that CoREST-mediated MYC stabilization plays a critical role in poor survival of melanoma patients (Fig. 2J).

The CoREST-complex regulates genes mediating post-transcriptional mRNA splicing in melanoma cells.

To gain insights into the functional roles of the CoREST-complex in cancer cells, we performed transcriptomic analysis by RNA-sequencing on three melanoma cell lines (A375, WM983B, and SK-MEL2) with RCOR1 knockdown (KD). Differentially expressed genes (DEGs) were identified by comparison with wildtype control cells. We found that decreased RCOR1 expression level induced more upregulated genes than down-regulated genes, which is consistent with its known function as a transcriptional repressor. However, a significant number of genes were also down-regulated in all three cell lines, suggesting a regulatory role of the CoREST-complex in transcriptional activation for a subset of genes (Fig. 3A).

Gene ontology analysis by Gene Set Enrichment Analysis (GSEA) paired with human Molecular Signature Database (MSigDB v2023.1.Hs) was performed to identify gene signatures commonly regulated by the CoREST-complex in the three melanoma cell lines. While several gene sets associated with immune and inflammation responses were enriched in upregulated genes, the most highly enriched gene sets in the down-regulated genes were divided into two functionally distinctive groups. One group of gene sets is known for their association with chromosome regulation, such as DNA replication, chromosome segregation, and sister chromatid segregation. Interestingly, the other group of gene sets is mainly associated with post-transcriptional RNA processing, such as ribonucleoprotein complex biogenesis and RNA splicing via transesterification (Fig. 3B and Supplementary Fig. S3).

Among the notably down-regulated genes common in the three RCOR1 KD melanoma cell lines, genes encoding several core components of spliceosome complexes (*SF1*, *SF3A1/2/3*, *SF3B5*, *SRSF5/10*, and *GEMIN4/7*), DEAD/H-box RNA helicases (*DDX21*, *DDX23*, *DDX49*, *DHX9*, and *DHX30*), nuclear RNA exosome complex (*EXOSC1*, *EXOSC2*, *EXOSC3*, *EXOSC8*, *EXOSC9*, and *EXOSC10*), and several small nuclear ribonucleoproteins (snRNPs) including small nucleolar ribonucleoproteins (snoRNPs) involved in both spliceosome and ribosome assembly and biogenesis, such as *NOL11*, *NOLC1*, *NOP56*, and *NOP58* were included (Fig. 3C). This suggests dysregulation in a broad range of post-transcriptional RNA processing steps by the RCOR1 KD in the melanoma cells. Computational analysis of our RNA-seq data confirmed widespread changes in mRNA isoform generation, which can be attributed to the decreased expression of RNA processing signature genes in the RCOR1-KD cells compared to control cells (Fig. 3D). For further analysis to corroborate the alternative splicing switching observed from the RNA-seq data analysis, we selected a set of genes (*PELO*, *STX1A*, and *FAM20C*) identified for their differential exon usage in the RCOR1-KD A375 cells, and experimentally verified their isoform switching using freshly prepared mRNA samples. For example, exon 2 of *PELO* was skipped as much as 83% while exon 6 of *STX1A* was retained

(53%) in the RCOR1-KD cells compared to the control cells (Fig. 3E). These observations suggest that CoREST-complex plays a role in alternative splicing by regulating the RNA processing genes.

The CoREST-complex regulates mRNA processing by increasing MYC stability.

Since the CoREST-complex promotes increased MYC protein expression (Fig. 1 and 2) and given the critical role of MYC in the regulation of core pre-mRNA splicing machinery (32-34), we performed CoREST-complex and MYC chromatin immunoprecipitation sequencing (ChIP-seq) analysis using anti-RCOR1 and anti-MYC antibodies in an A375 melanoma cell line. We found that 30% of the RCOR1 ChIP-seq peaks (1,966 out of 6,461 peaks) within gene transcription regulatory regions, defined as ±2.0 kb from the transcription start site (TSS), were also co-localized with MYC ChIP-seq peaks (Fig. 4A). The intervals between the two sequence motifs were searched. Most RCOR1- and MYC-binding motifs were located within a span of a nucleosome length of DNA (approximately 180 bp), which was also true in two different cancer type cell lines: lymphoblast (K562) and breast cancer (MCF7) (Fig. 4B). To explore the possibility of RCOR1 cooperation with MYC in regulation of RNA processing, we performed a gene ontology (GO) term analysis using GOMo (Gene Ontology for Motifs) program (35) to identify biological processes potentially regulated by the genes controlled by the RCOR1 motifs. We found that the majority of gene sets regulated by the RCOR1-binding motifs are involved in the biological role of RNA processing, including RNA splicing and ribosome biogenesis (Fig. 4C).

To further corroborate the role of CoREST-complex in transcriptional regulation of RNA processing genes, both RCOR1- and MYC-binding peaks in the proximal regulatory regions of genes known for regulating RNA processing (GO:0006396) were determined. Only a subset of genes (62 out of 863 genes, 7.2%) harbors the RCOR1-binding motifs, while 151 genes (17.5%) harbor MYC-binding peaks (Fig. 4D and Supplementary Table S1). Interestingly, all the

RCOR1-bound gene promoter regions are also co-occupied by MYC. Experimental validations of the co-binding of the CoREST-complex and MYC by Re-ChIP assay (Fig. 4E) at the proximal regulatory regions of the RNA processing genes selected from the list of 62 genes and their decreased expressions in the RCOR1-KD melanoma cells by RT-PCR assay (Fig. 4F) indicate that the CoREST-complex and MYC co-regulate the transcriptional activation of a subset of genes involved in RNA processing in cancer cells.

There are also significant correlations in expression levels between RCOR1 and the subset of RNA processing genes controlled by CoREST-complex in cancer patients including melanoma. Among the 62 genes whose expression was controlled by CoREST-complex and MYC, 22 genes were positively correlated to *RCOR1* expression with statistical significance, whereas only 8 genes were inversely correlated in melanoma patient samples (TCGA SKCM). Very similar patterns were also observed when analyzing the TCGA pan-cancer data set, showing that *DHX9* and *NOLC1* were the top two genes positively correlated with RCOR1 expression level (Fig. 4G). Amongst the 22 genes, *NOLC1*, encoding nucleolar coiled-body phosphoprotein 1 (NOPP140) showed significantly poor survival in the melanoma patient group with high expression compared to the group with low expression (Fig. 4H). Depletion of NOPP140 in melanoma cells induced significant growth inhibition, phenocopying the RCOR1 KD, and ectopic expression of HA-tagged NOPP140 in the RCOR1-KD cells showed partial phenotype rescue (Fig. 4I), suggesting that NOPP140, a key protein for Cajal body organization and pre-mRNA splicing fidelity (36,37), is a downstream effector of the CoREST-complex-MYC pathway in melanoma. Taken together, these data obtained from melanoma cell lines and human patient samples strongly suggest distinctive roles of CoREST-complex in transcriptional activation of the genes involved in RNA processing through PTM-mediated MYC stabilization in cancer cells.

Discussion

In this study, we uncovered a novel role of the CoREST-complex in the regulation of MYC protein in melanoma cells. We have identified that CoREST-complex regulates the MYC stability through site-specific deacetylation of lysine (K) residues and promotes dysregulation of post-transcriptional mRNA splicing. Together with recent studies by other groups, revealing the critical roles of the CoREST-complex in regulating cellular plasticity and therapy resistance in melanoma and endocrine-resistant breast cancer (38,39), our study highlights the complex's important roles in melanoma cells, suggesting a viable therapeutic target.

The CoREST-complex is unique among the class I HDAC1/2-containing chromatin-remodeling complexes (CoREST, SIN3, NuRD, and MiDAC) due to its co-existence with HDAC1/2 and LSD1 in the complex (of note, the NuRD complex also contains LSD1 sub-stoichiometrically). While these complexes are generally known as gene transcription regulators that modify post-translational histone acetylation and methylation, our study revealed that the CoREST complex can regulate the stability of the non-histone protein MYC via deacetylation of specific K residues. The role of MYC acetylation is dubious and the acetylation at different K residues affects its stability differentially in a cell type-dependent manner. This HAT-mediated MYC acetylation and its cellular effects are counterbalanced by endogenous HDACs in normal cells. According to the study by Hurd et al., acetylation of three K residues (K148, K157, and K323) is conserved in a diverse set of human cancer cell lines (24). These residues are differentially targeted by p300 (K148 and K157) and GCN5 (K323) and affect MYC stability differentially; p300-mediated AcK148 and AcK157 lead to unstable MYC, while GCN5-dependent AcK323 results in more stable MYC (24). However, all the five deacetylation targets (AcK148, AcK157, AcK275, AcK289, and AcK323) identified in our study showed increased stability in melanoma cells when treated with the CoREST-complex inhibitor. Unlike the HATs for site-specific acetylation on MYC stability, this observation suggests that HDAC1/2 in the CoREST complex indiscriminately deacetylate these AcKs, leading to stabilized MYC in melanoma cells.

MYC's regulatory functions in specific genetic programs heavily rely on its cofactor interactions, such as those with p300/CBP and TRRAP (40). The specific genetic programs regulated by MYC can vary significantly depending on cell type and availability of different cofactors, allowing for context-specific gene regulation. Likewise, MYC-regulated genetic programs mediated by HDAC-containing complexes, such as CoREST, NuRD, and SIN3A, are not well-defined in cancer cells. Nevertheless, in this study, we observed that gene sets under the direct transcriptional control of the CoREST-complex include those involved in mRNA splicing and ribosome biogenesis. This result is consistent with the recent identification of site-specific acetylated MYC-mediated transcriptionally activated gene sets in Rat1a and MCF10A cells: e.g., KEGG_SPLICEOSOME by the acetylated MYC-K323 and KEGG_RIBOSOME by the acetylated MYC-K148 (24). These study results support the idea that one of the primary functions of the CoREST-complex is to regulate post-transcriptional mRNA splicing through increasing MYC stability in melanoma cells.

Our ChIP-seq and gene ontology (GO) analyses of genes controlled by both the CoREST-complex and MYC also identified a subset of genes directly regulated by these factors in melanoma cells. This subset of RNA processing genes includes many RNA helicases such as DEAD/H-Box proteins, which play important roles in mRNA splicing (41), and nuclear exosome complexes, which are important for 3' processing of various RNA species and RNA quality control (42). Interestingly, the majority of the 62 genes co-occupied by both the CoREST-complex and MYC encode snRNP and snoRNP complex-interacting proteins that are known to critically mediate RNA spliceosome and ribosome activity. Notably, several proteins known for regulating RNA methylation, such as *ALKBH5*, *BCDIN3D*, *METTL16*, *MRM1*, *NOLC1*, *TFB2M*, *TRMT12*, and *ZCCHC4* (Supplementary Table S1) were included, suggesting that the CoREST-complex may also play a role in RNA methylation in melanoma. Particularly, the NOPP140 protein, encoded by the *NOLC1* gene whose expression is under direct control of both the CoREST-complex and MYC in melanoma cells, plays a crucial role in RNA methylation,

particularly in the 2'-O-methylation of small nuclear RNAs (snRNAs) and ribosomal RNAs. NOPP140 is essential for concentrating small Cajal body-specific ribonucleoproteins (scaRNPs) in Cajal bodies (36). This localization is critical for the 2'-O-methylation of spliceosomal snRNAs, such as U1, U2, U5, and U12 snRNAs, which is crucial for maintaining pre-mRNA splicing fidelity. Moreover, the observation of a positive expression correlation between NOPP140 (NOLC1) and CoREST (RCOR1), and the poor survival of melanoma patients with increased NOPP140 expression, suggest that the CoREST-complex-MYC-NOPP140 pathway may be a therapeutic target and a possible prognostic marker for melanoma. This warrants further research on the pathogenic role of NOPP140 in cancer-specific RNA processing and mRNA splicing variant formation.

Methods

Cell culture: The cell lines used in this study were cultured in DMEM supplemented with 10% FBS and 1% penicillin/streptomycin at 37°C with 5% CO2 in a humidified incubator. WM983B and 1205Lu cells were obtained from M. Herlyn (The Wistar Institute). All other cells were purchased from ATCC and tested to be free of mycoplasma.

Plasmid construction for stable cell line generation: The knockdowns were performed using lentiviral plasmid pLKO.1-TRC (Addgene_10878). The plasmid was digested with EcoRI (NEB, USA) and AgeI (NEB, USA). The annealed shRNA oligos for the target genes were cloned into the EcoRI and AgeI sites of pLKO.1 vector and ligated with Ligase mixture (TAKARA, Japan). The shRNA clones were confirmed by Sanger sequencing.

For the ectopic expression of proteins, the genes were PCR amplified from cDNA, digested with BamHI (NEB, USA) and NotI (NEB, USA), and cloned into pCDH-EF1α-puro vector under the EF1α promoter and puromycin selection marker with HA or FLAG tag. The clones were confirmed by Sanger sequencing (GENEWIZ, NJ USA). The RCOR1 clone was purchased from

a commercial company (GeneCopoeia_ U0745). The mutant MYC clones were amplified with primers containing the mutant amino acid sequences from the WT MYC clones and confirmed by Sanger sequencing (GENEWIZ, NJ USA). For the construction of lentiviral particles, Lenti-X-293T cells were transiently transfected with ORF or shRNA vectors with packaging plasmids Pax2, PMD2.G at 3:2:1 using Lipofectamine 2000 (Invitrogen, USA). The viral particles were harvested 48 and 72 hrs post-transfection and filtered through a 0.45μm filter. Cells were transduced with viral particles and selected with 1μM puromycin for at least 72 hrs.

Chemicals: Corin was synthesized in the laboratory of P.A. Cole (Harvard Medical School). MS275, GSK2879552, and P300/CBP inhibitor A-485 were purchased from MedChem Express (Monmouth Junction, NJ USA).

RNA sequencing and analysis: Total RNA was extracted using TRIzol reagent from the melanoma cells (A375, WM983B, and SK-MEL2), stable RCOR1 knockdown and control, as well as Corin-treated and DMSO control cells. RNA was processed with the Ribo-Zero rRNA Removal Kit (Illumina) and further processed using TruSeq RNA Sample Prep Kit (Illumina). Sequencing libraries were prepared following the manufacturer's recommendations. Samples were barcoded and sequenced using standard Illumina chemistry at GENEWIZ. The sequence reads were trimmed to remove possible adapter sequences and nucleotides with poor quality using Trimmomatic v.0.39. The trimmed reads were mapped to the Homo sapiens GRCh39 reference genome available on ENSEMBL using STAR aligner v.2.7.1b. Gene hit counts and unique gene hit counts were calculated using FeatureCounts from the Subread package v.2.0.3. Gene counts were further analyzed to test for differential expression using R package DESeq2 (43) contrasting by RCOR1 KD or Corin treatment. For GSEA analysis, the differentially expressed genes (DEGs) between RCOR1 knockdown and control in each cell line were chosen up to 10 reads, and log2 fold changes between the samples were ranked from top to bottom. The dataset was analyzed using the software program GSEA4.3.2 downloaded from

Broad Institute, and the enriched gene sets were identified based on human Molecular Signature Database (MSigDB v2023.1.Hs). Differential exon usage analysis was performed using R package DEXseq (44) by following standard protocol.

ChIP sequencing and analysis: ChIP assay was performed as described previously (45). Briefly, cells were crosslinked with 1% formaldehyde for 10 min, and the reaction was stopped with a final concentration of 0.137M Glycine for 5 min followed by two washes with ice-cold PBS. Cell nuclei were extracted with buffer 1 (10 mM HEPES [pH 6.5], 0.25% Triton X-100, 10 mM EDTA, 0.5 mM EGTA, and 1 mM PMSF) and buffer 2 (10 mM HEPES [pH 6.5], 200 mM NaCl, 1 mM EDTA, 0.5 mM EGTA, and 1 mM PMSF). The nuclei pellet was resuspended in RIPA buffer and sonicated to a range of 300bp~500bp with M220 focused-ultrasonicator (Covaris, USA). The sonicated chromatin was incubated with 5µg of indicated antibodies followed by A/G magnetic beads (ThermoFisher, USA) and incubated overnight at 4°C with overhead rotation. The complex was washed once with buffer-1 (0.1% SDS, 1% T-X-100, 2mM EDTA, 150mM NaCl, 20mM Tris-HCl (pH 8.1)) for 10min, twice with buffer-2 (0.1% SDS, 1X T-X-100, 2mM EDTA, 500mM NaCl, 20mM Tris-HCl (pH 8.1)), and twice with buffer-3 (0.25M LiCl, 1%NP-40, 1% Sodium deoxycholate, 1mM EDTA, 10mM Tris-HCl), and finally twice with 1X TE buffer. 10% of the sonicated chromatin was used as input. ChIP samples were reverse crosslinked with proteinase K for 12h at 65°C. The DNA was purified by the phenol/chloroform method and sequenced using standard Illumina chemistry at GENEWIZ. We performed a preliminary quality check of the ChIP-seq data sets using FASTQC, a quality control tool for high throughput sequence data, then aligned the reads to the Homo sapiens genome and annotations version GRCh39 available on ENSEMBL using the standard protocol and parameters from STAR aligner v2.7.1b. We called peaks from the aligned read files for both RCOR1 and MYC datasets using MACS version 3 and "callpeaks" function (46), and kept all peaks using the IgG dataset as control with all standard parameters except for "-q 0.01" for the

downstream analysis. We further identified sites with peaks in common between the RCOR1 and MYC using INTERVENE (47).

Other bioinformatics analysis: Gene ontology (GO) term analysis with RCOR1 and MYC peak sequences were performed using PANTHER (48) over-representation analysis and GO Ontology database released May 10, 2023.

Re-ChIP analysis: The chromatin for ChIP-re-ChIP was prepared as above for ChIP-Seq. After performing ChIP, the immunoprecipitated chromatin was eluted with an elution buffer (1mM EDTA, 1%SDS, 10mM DTT) and incubated at 65°C for 10min. The eluted product was diluted ten times in the RIPA buffer excluding SDS and divided into two parts. To one part, the antibody-beads complex was added, and to another half, only beads were added to use as a control and incubated overnight with overhead rotation at 4ºC. The chromatin was washed again with buffer-1, buffer-2, buffer-3, and TE buffer as mentioned above. The DNA was isolated by incubating the complex with proteinase K for 12h at 65°C and purified with phenol/chloroform and ethanol precipitation.

Proximity ligation assay: PLA (DuoLink, Sigma) was performed according to the manufacturer's instructions. Briefly, cells were fixed with 4% PFA for 10 min followed by permeabilization with 0.5% T-X-100 for 10 min. Cells were blocked in PLA blocking buffer for 30 min at 37°C and incubated with primary antibodies diluted in antibody dilution buffer for 1h at RT. Cells were washed twice in wash buffer A for 5 min and then incubated with PLA probes (rabbit (+) and mouse (-)) for 1h at 37°C. After washing twice with wash buffer A, the probes were ligated for 30 min at 37°C. The ligated product was amplified at 37°C for 100 min for fluorescent labeling. Cells were washed with wash buffer B for 10 min each followed by a brief wash with 0.01X buffer B. Cells were mounted using In Situ Mounting Medium with DAPI, and the coverslip on the slide was sealed with nail polish. Images were acquired with the NIS-Elements Viewer microscope.

Cell growth assay: Cell growth assay was performed using CellTiter-Glo 2.0 reagent (Promega, USA) according to the manufacturer's instructions. Briefly, cells were grown in 96-well plates and a volume of CellTiter-Glo 2.0 reagent was added. The content was mixed on an orbital shaker for 2 min to lyse the cells and then incubated for 10 min at room temperature to stabilize the luminescent signal.

Apoptosis assay: Cultured cells were trypsinized and washed two times with cold BioLegend Cell Staining Buffer and then resuspend with 500 ul Annexin V Binding Buffer. Add 5ul of FITC-conjugated Annexin V. Then, cells were stained with a viability dye, 7-AAD. After staining and washing, cells were acquired on a LSRFortessa flow cytometer (BD, USA) and analyzed using Diva software (BD, USA).

Recombinant protein expression in E. coli: For protein expression in E. coli BL21 DE3, a single colony was grown overnight at 4°C as a starter culture. The starter culture was transferred to a larger volume of LB media until the OD reached 0.4~0.6 (~3 hrs). For induction of protein expression, 1mM IPTG was added to the media and incubated for at least 3 hrs. The cells were centrifuged at 4000 RPM for 10 min and the pellet was stored at -30°C until use. For the isolation of inclusion bodies (IBs), the pellet was resuspended in xFactor buffer (Takara, USA) and rotated at 4°C for 30 min, and the IBs were recovered by centrifugation at 12000 RPM for 20min. The pellet was again resuspended in lysis buffer (8M urea, 50mM sodium phosphate monobasic, 300mM sodium chloride (NaCl), 10mM imidazole, and 10% T-X-100, pH8) and sonicated 6 times for 15 sec ON and 15 sec OFF with 30 Amplitude. The sonicated cells were centrifuged for 30 min at 12000 RPM and the supernatant collected. The Ni-NTA beads were washed with the lysis buffer in a column and the cell lysate was added to the resin. The cell lysate was allowed to drain from the column by gravity. The resin was washed with a wash buffer (8M urea, 50mM sodium phosphate monobasic, 300mM NaCl, 20mM Imidazole, pH8). The protein was eluted with an elution buffer (8M urea, 50mM sodium phosphate

monobasic, 300mM NaCl, 250mM Imidazole, pH8). To remove the imidazole and refold the protein for downstream applications, the protein was dialyzed (Slide-A-Lyzer Dialysis Cassettes, Thermo Fisher, USA) against decreasing concentrations of urea and finally against 50mM Tris and 150mM NaCl buffer. The concentration of protein was measured with the BCA method and stored at -80°C in the storage buffer (50mM Tris, 150mM NaCl, 5mM DTT, 20% glycerol).

Co-IP and immunoblotting: Cells were lysed with 1X non-denaturing lysis buffer (20mM Tris, 137mM NaCl, 1% NP-40, 0.2mM EDTA) and rotated for 30 min at 4°C. The cell lysate was centrifuged at 13,000 RPM for 15 min and supernatant was collected. The soluble fraction was incubated with indicated antibodies at 4°C overnight followed by incubation with A/G magnetic beads (Fisher Scientific, USA) for at least 4 hours. The immunoprecipitates were washed 5 times with lysis buffer and eluted in 2X SDS buffer by boiling for 10 min at 100°C. For western blot, the cells were lysed in RIPA buffer (10mM Tris, 1mM EDTA, 0.5mM EGTA, 1% T-X-100, 0.1% sodium deoxycholate, 0.1% SDS and 140mM NaCl) followed by incubation at 4°C with overhead rotation. The cell debris was removed by centrifugation. The protein was quantified by BCA assay (Fisher Scientific, USA). Protein was resolved on SDS-PAGE and immunoblotting was carried out with indicated antibodies.

RT-PCR: RNA was isolated by TRIzol reagent (Life Technologies, USA) according to the manufacturer's instructions followed by DNase I (Invitrogen, USA) treatment. RNA was purified by phenol/chloroform and dissolved in nuclease-free water. RNA was reverse transcribed by SuperScript III first-strand synthesis system (ThermoFisher Scientific, USA) or cDNA synthesis Kit (Applied Biosystems, USA). The cDNA was subjected to semiquantitative RT-PCR using SYBR green master mix (TOYOBO, Japan). For the exon usage confirmation, the primers were designed based on RNA-seq exon usage regions and amplified by KOD PCR master mix (TOYOBO, Japan). The PCR products were run on agarose gel. The list of primers used in the PCR is indicated in the Supplementary Table S2.

Ubiquitination analysis: Cells were treated with Corin for 24h followed by 10μM of MG132 for 4h. Cell lysates were prepared with the lysis buffer (1% SDS, 0.5% Sodium deoxycholate, 1% Triton-X-100, 20mM NAP, and 150mM NaCl). The lysates were sonicated for 30 sec and boiled for 15 min at 95°C. The lysates were diluted in the RIPA buffer and centrifuged at 12000 RPM for 20 min. The supernatant was incubated with FLAG antibody and A/G magnetic beads at 4°C overnight. After washing, the proteins were eluted by 2X SDS sample buffer at 95°C for 5 min. The MYC ubiquitination was determined by western blotting with ubiquitin antibody.

Statistics and reproducibility: Student's t-test (two-sided) was applied and considered significant when $p<0.05$. All results are shown as mean with s.d. of at least three biological replicates. GraphPad Prism software v9.5.1. was for statistical analyses.

Data availability: Raw RNA-seq and ChIP-seq files have been deposited in the National Center for Biotechnology Information BioProject (access code: PRJNA996569). ChIP-sequencing data for K562 (access codes: 84245 (H3K27Ac), 45560 (MYC), 01906(RCOR1)) and MCF7 (access codes: 8183 (MYC), 63457 (RCOR1)) cell lines were downloaded from Cistrome DB (49). All other raw data are available upon request from the corresponding author.

Authors' Disclosures

B. Ryu reports grants from NIH/NCI the New Jersey Health Foundation during the conduct of the study. J. L Zakrzewski reports grants from NIH/NCI, the New Jersey Health Foundation, and the Children's Leukemia Research Association and Hyundai Hope on Wheels. J. Shin reports grants from NIH/NCI.

Authors' Comtributions

A.A. Khan: Conceptualization, investigation, data curation, formal analysis, validation, methodology, visualization, writing–review and editing. **A.A. Aptekmann:** Investigation, data

curation, formal analysis, validation, methodology, visualization, writing–review and editing. **J. Byun:** investigation, data curation, formal analysis, validation, methodology, visualization, writing–review and editing. **D. Min:** investigation, validation, methodology, writing–review and editing. **M.C. Povelaitis:** investigation, validation, writing–review and editing. **J. Shin:** Writing–review and editing. **J.L. Zakrzewski:** Writing–review and editing. **B. Ryu:** Conceptualization, resources, data curation, formal analysis, supervision, funding acquisition, validation, methodology, visualization, writing–original draft, writing–review and editing.

Acknoledgement

The authors would like to express our sincere gratitude to Philip A Cole at Harvard Medical School and Brigham and Women's Hospital for his invaluable contributions and research materials that greatly enriched this study. This work was supported by an NCI grant (R01CA212639) and in part a research grant from the New Jersey Health Foundation.

References:

1. Andres ME, Burger C, Peral-Rubio MJ, Battaglioli E, Anderson ME, Grimes J*, et al.* CoREST: a functional corepressor required for regulation of neural-specific gene expression. Proc Natl Acad Sci U S A **1999**;96(17):9873-8 doi 10.1073/pnas.96.17.9873.
2. You A, Tong JK, Grozinger CM, Schreiber SL. CoREST is an integral component of the CoREST- human histone deacetylase complex. Proc Natl Acad Sci U S A **2001**;98(4):1454-8 doi 10.1073/pnas.98.4.1454.
3. Shi Y, Lan F, Matson C, Mulligan P, Whetstine JR, Cole PA*, et al.* Histone demethylation mediated by the nuclear amine oxidase homolog LSD1. Cell **2004**;119(7):941-53 doi 10.1016/j.cell.2004.12.012.
4. Humphrey GW, Wang Y, Russanova VR, Hirai T, Qin J, Nakatani Y*, et al.* Stable histone deacetylase complexes distinguished by the presence of SANT domain proteins CoREST/kiaa0071 and Mta-L1. J Biol Chem **2001**;276(9):6817-24 doi 10.1074/jbc.M007372200.
5. Saijo K, Winner B, Carson CT, Collier JG, Boyer L, Rosenfeld MG*, et al.* A Nurr1/CoREST pathway in microglia and astrocytes protects dopaminergic neurons from inflammation-induced death. Cell **2009**;137(1):47-59 doi 10.1016/j.cell.2009.01.038.
6. Saleque S, Kim J, Rooke HM, Orkin SH. Epigenetic regulation of hematopoietic differentiation by Gfi-1 and Gfi-1b is mediated by the cofactors CoREST and LSD1. Mol Cell **2007**;27(4):562-72 doi 10.1016/j.molcel.2007.06.039.
7. Kim SA, Zhu J, Yennawar N, Eek P, Tan S. Crystal Structure of the LSD1/CoREST Histone Demethylase Bound to Its Nucleosome Substrate. Mol Cell **2020**;78(5):903-14 e4 doi 10.1016/j.molcel.2020.04.019.
8. Pilotto S, Speranzini V, Tortorici M, Durand D, Fish A, Valente S*, et al.* Interplay among nucleosomal DNA, histone tails, and corepressor CoREST underlies LSD1-mediated H3 demethylation. Proc Natl Acad Sci U S A **2015**;112(9):2752-7 doi 10.1073/pnas.1419468112.
9. Kim SA, Chatterjee N, Jennings MJ, Bartholomew B, Tan S. Extranucleosomal DNA enhances the activity of the LSD1/CoREST histone demethylase complex. Nucleic Acids Res **2015**;43(10):4868-80 doi 10.1093/nar/gkv388.
10. Rivera C, Lee HG, Lappala A, Wang D, Noches V, Olivares-Costa M*, et al.* Unveiling RCOR1 as a rheostat at transcriptionally permissive chromatin. Nat Commun **2022**;13(1):1550 doi 10.1038/s41467-022-29261-0.
11. Bennesch MA, Segala G, Wider D, Picard D. LSD1 engages a corepressor complex for the activation of the estrogen receptor alpha by estrogen and cAMP. Nucleic Acids Res **2016**;44(18):8655-70 doi 10.1093/nar/gkw522.
12. Metzger E, Wissmann M, Yin N, Muller JM, Schneider R, Peters AH*, et al.* LSD1 demethylates repressive histone marks to promote androgen-receptor-dependent transcription. Nature **2005**;437(7057):436-9 doi 10.1038/nature04020.
13. Wang J, Scully K, Zhu X, Cai L, Zhang J, Prefontaine GG*, et al.* Opposing LSD1 complexes function in developmental gene activation and repression programmes. Nature **2007**;446(7138):882-7 doi 10.1038/nature05671.
14. Dang CV. MYC on the path to cancer. Cell **2012**;149(1):22-35 doi 10.1016/j.cell.2012.03.003.
15. Vita M, Henriksson M. The Myc oncoprotein as a therapeutic target for human cancer. Semin Cancer Biol **2006**;16(4):318-30 doi 10.1016/j.semcancer.2006.07.015.
16. Amati B, Sanchez-Arevalo Lobo VJ. MYC degradation: deubiquitinating enzymes enter the dance. Nat Cell Biol **2007**;9(7):729-31 doi 10.1038/ncb0707-729.
17. Farrell AS, Sears RC. MYC degradation. Cold Spring Harb Perspect Med **2014**;4(3) doi 10.1101/cshperspect.a014365.

18. Gabay M, Li Y, Felsher DW. MYC activation is a hallmark of cancer initiation and maintenance. Cold Spring Harb Perspect Med **2014**;4(6) doi 10.1101/cshperspect.a014241.
19. Patel JH, Du Y, Ard PG, Phillips C, Carella B, Chen CJ*, et al.* The c-MYC oncoprotein is a substrate of the acetyltransferases hGCN5/PCAF and TIP60. Mol Cell Biol **2004**;24(24):10826-34 doi 10.1128/MCB.24.24.10826-10834.2004.
20. Zhang K, Faiola F, Martinez E. Six lysine residues on c-Myc are direct substrates for acetylation by p300. Biochem Biophys Res Commun **2005**;336(1):274-80 doi 10.1016/j.bbrc.2005.08.075.
21. Lynch JT, Somerville TD, Spencer GJ, Huang X, Somervaille TC. TTC5 is required to prevent apoptosis of acute myeloid leukemia stem cells. Cell Death Dis **2013**;4(4):e573 doi 10.1038/cddis.2013.107.
22. Marshall GM, Liu PY, Gherardi S, Scarlett CJ, Bedalov A, Xu N*, et al.* SIRT1 promotes N-Myc oncogenesis through a positive feedback loop involving the effects of MKP3 and ERK on N-Myc protein stability. PLoS Genet **2011**;7(6):e1002135 doi 10.1371/journal.pgen.1002135.
23. Nascimento EM, Cox CL, MacArthur S, Hussain S, Trotter M, Blanco S*, et al.* The opposing transcriptional functions of Sin3a and c-Myc are required to maintain tissue homeostasis. Nat Cell Biol **2011**;13(12):1395-405 doi 10.1038/ncb2385.
24. Hurd M, Pino J, Jang K, Allevato MM, Vorontchikhina M, Ichikawa W*, et al.* MYC acetylated lysine residues drive oncogenic cell transformation and regulate select genetic programs for cell adhesion-independent growth and survival. Genes Dev **2023**;37(19-20):865-82 doi 10.1101/gad.350736.123.
25. Spain L, Coulton A, Lobon I, Rowan A, Schnidrig D, Shepherd STC*, et al.* Late-Stage Metastatic Melanoma Emerges through a Diversity of Evolutionary Pathways. Cancer Discov **2023**;13(6):1364-85 doi 10.1158/2159-8290.CD-22-1427.
26. Menssen A, Hydbring P, Kapelle K, Vervoorts J, Diebold J, Luscher B*, et al.* The c-MYC oncoprotein, the NAMPT enzyme, the SIRT1-inhibitor DBC1, and the SIRT1 deacetylase form a positive feedback loop. Proc Natl Acad Sci U S A **2012**;109(4):E187-96 doi 10.1073/pnas.1105304109.
27. Garcia-Sanz P, Quintanilla A, Lafita MC, Moreno-Bueno G, Garcia-Gutierrez L, Tabor V*, et al.* Sin3b interacts with Myc and decreases Myc levels. J Biol Chem **2014**;289(32):22221-36 doi 10.1074/jbc.M113.538744.
28. Kurland JF, Tansey WP. Myc-mediated transcriptional repression by recruitment of histone deacetylase. Cancer Res **2008**;68(10):3624-9 doi 10.1158/0008-5472.CAN-07-6552.
29. Kalin JH, Wu M, Gomez AV, Song Y, Das J, Hayward D*, et al.* Targeting the CoREST complex with dual histone deacetylase and demethylase inhibitors. Nat Commun **2018**;9(1):53 doi 10.1038/s41467-017-02242-4.
30. Deng W, Wang C, Zhang Y, Xu Y, Zhang S, Liu Z*, et al.* GPS-PAIL: prediction of lysine acetyltransferase-specific modification sites from protein sequences. Sci Rep **2016**;6:39787 doi 10.1038/srep39787.
31. Lasko LM, Jakob CG, Edalji RP, Qiu W, Montgomery D, Digiammarino EL*, et al.* Discovery of a selective catalytic p300/CBP inhibitor that targets lineage-specific tumours. Nature **2017**;550(7674):128-32 doi 10.1038/nature24028.
32. Koh CM, Bezzi M, Low DH, Ang WX, Teo SX, Gay FP*, et al.* MYC regulates the core pre-mRNA splicing machinery as an essential step in lymphomagenesis. Nature **2015**;523(7558):96-100 doi 10.1038/nature14351.
33. Lu SX, De Neef E, Thomas JD, Sabio E, Rousseau B, Gigoux M*, et al.* Pharmacologic modulation of RNA splicing enhances anti-tumor immunity. Cell **2021**;184(15):4032-47 e31 doi 10.1016/j.cell.2021.05.038.

34. Phillips JW, Pan Y, Tsai BL, Xie Z, Demirdjian L, Xiao W, *et al.* Pathway-guided analysis identifies Myc-dependent alternative pre-mRNA splicing in aggressive prostate cancers. Proc Natl Acad Sci U S A **2020**;117(10):5269-79 doi 10.1073/pnas.1915975117.
35. Buske FA, Boden M, Bauer DC, Bailey TL. Assigning roles to DNA regulatory motifs using comparative genomics. Bioinformatics **2010**;26(7):860-6 doi 10.1093/bioinformatics/btq049.
36. Bizarro J, Deryusheva S, Wacheul L, Gupta V, Ernst FGM, Lafontaine DLJ, *et al.* Nopp140-chaperoned 2'-O-methylation of small nuclear RNAs in Cajal bodies ensures splicing fidelity. Genes Dev **2021**;35(15-16):1123-41 doi 10.1101/gad.348660.121.
37. Courchaine E, Gelles-Watnick S, Machyna M, Straube K, Sauyet S, Enright J, *et al.* The coilin N-terminus mediates multivalent interactions between coilin and Nopp140 to form and maintain Cajal bodies. Nat Commun **2022**;13(1):6005 doi 10.1038/s41467-022-33434-2.
38. Garcia-Martinez L, Adams AM, Chan HL, Nakata Y, Weich N, Stransky S, *et al.* Endocrine resistance and breast cancer plasticity are controlled by CoREST. Nat Struct Mol Biol **2022**;29(11):1122-35 doi 10.1038/s41594-022-00856-x.
39. Wu M, Hanly A, Gibson F, Fisher R, Rogers S, Park K, *et al.* The CoREST repressor complex mediates phenotype switching and therapy resistance in melanoma. J Clin Invest **2024**;134(6) doi 10.1172/JCI171063.
40. Nikiforov MA, Chandriani S, Park J, Kotenko I, Matheos D, Johnsson A, *et al.* TRRAP-dependent and TRRAP-independent transcriptional activation by Myc family oncoproteins. Mol Cell Biol **2002**;22(14):5054-63 doi 10.1128/MCB.22.14.5054-5063.2002.
41. Chang TH, Tung L, Yeh FL, Chen JH, Chang SL. Functions of the DExD/H-box proteins in nuclear pre-mRNA splicing. Biochim Biophys Acta **2013**;1829(8):764-74 doi 10.1016/j.bbagrm.2013.02.006.
42. Kilchert C, Wittmann S, Vasiljeva L. The regulation and functions of the nuclear RNA exosome complex. Nat Rev Mol Cell Biol **2016**;17(4):227-39 doi 10.1038/nrm.2015.15.
43. Anders S, Reyes A, Huber W. Detecting differential usage of exons from RNA-seq data. Genome Res **2012**;22(10):2008-17 doi 10.1101/gr.133744.111.
44. Love MI, Huber W, Anders S. Moderated estimation of fold change and dispersion for RNA-seq data with DESeq2. Genome Biol **2014**;15(12):550 doi 10.1186/s13059-014-0550-8.
45. Khan AA, Ham SJ, Yen LN, Lee HL, Huh J, Jeon H, *et al.* A novel role of metal response element binding transcription factor 2 at the Hox gene cluster in the regulation of H3K27me3 by polycomb repressive complex 2. Oncotarget **2018**;9(41):26572-85 doi 10.18632/oncotarget.25505.
46. Zhang Y, Liu T, Meyer CA, Eeckhoute J, Johnson DS, Bernstein BE, *et al.* Model-based analysis of ChIP-Seq (MACS). Genome Biol **2008**;9(9):R137 doi 10.1186/gb-2008-9-9-r137.
47. Khan A, Mathelier A. Intervene: a tool for intersection and visualization of multiple gene or genomic region sets. BMC Bioinformatics **2017**;18(1):287 doi 10.1186/s12859-017-1708-7.
48. Mi H, Lazareva-Ulitsky B, Loo R, Kejariwal A, Vandergriff J, Rabkin S, *et al.* The PANTHER database of protein families, subfamilies, functions and pathways. Nucleic Acids Res **2005**;33(Database issue):D284-8 doi 10.1093/nar/gki078.
49. Zheng R, Wan C, Mei S, Qin Q, Wu Q, Sun H, *et al.* Cistrome Data Browser: expanded datasets and new tools for gene regulatory analysis. Nucleic Acids Res **2019**;47(D1):D729-D35 doi 10.1093/nar/gky1094.

Figure legends:

Fig. 1. MYC binding to CoREST-complex stabilizes MYC from proteolytic degradation in melanoma cells. A) Proximity ligation assay between MYC and each core component of CoREST-complex (RCOR1, HDAC1/2, and LSD1) in WM983B melanoma cells. **B)** Co-immunoprecipitation assays showing MYC interaction with CoREST-complex. *In vitro* binding was performed by incubating purified His-tagged full-length MYC protein with MeWo cell lysate. MYC binding in cells (HEK293T) was performed by expressing FLAG-tagged full-length MYC and HA-tagged RCOR1. **C)** Immunoblots of MYC levels in melanoma cells with RCOR1 knockdown (KD) and proteasome inhibitor MG132 treatment (10 μM, 4 hrs). **D)** Immunoblots of MYC in cells overexpressing HA-tagged RCOR1. **E)** Positive correlation in expression levels between RCOR1 and MYC proteins in a panel of 14 melanoma cell lines. **F)** Semi-quantitative RT-PCR analysis of six MYC target genes selected from Hallmark MYC Targets V1 gene set (MSigDB) in RCOR1-KD and control cells. **G**) Semi-quantitative RT-PCR analysis of MYC transcript levels in six melanoma cell lines with RCOR1 KD compared to those of control cells. **H)** Flow cytometry analysis of melanoma cells (WM983B) with knockdown of RCOR1, LSD1, and MYC genes via lentiviral shRNA, respectively.

Fig. 2. Site-specific deacetylation of MYC by CoREST-complex stabilizes MYC protein in melanoma. A) Pharmacologic inhibition of CoREST-complex by HDAC1/2 and LSD1 dual inhibitor Corin, Class I HDAC inhibitor MS275 (HDACi), LSD1 inhibitor GSK2879552 (LSD1i), and combination of MS275 and GSK2879552 (HDACi + LSD1i) in WM983B cells showing a dose-dependent MYC level decrease by Corin. Cells were treated with the indicated doses of each inhibitor for 36 hrs. Data are the means and s.d. of three independent immunoblot experiments. **B)** Representative images of MYC immunoblot experiments (A). **C)** Site-directed

mutagenesis analysis of mutant MYC in WM983B melanoma cells. Each N-terminal HA-tagged mutant MYC at the predicted Lys sites was ectopically expressed in WM983B cells and treated with Corin at doses of 0.0, 0.25, 0.5, and 1.0 μM for 36 hrs. The mutant MYC proteins were immunoblotted with an anti-HA antibody. Quantification analysis of the ectopically expressed mutant MYC proteins using ImageJ identified potential Lys residues targeted by HDAC1/2 in the CoREST-complex. **D)** Mutagenesis assay showing the 5x-mutant MYC (MYC-DR) and wildtype-MYC (MYC-WT) levels in RCOR1-KD and control WM983B cells. A representative immunoblots assay (upper panel) and quantification (lower panel) from biological triplicates. **E)** Quantification of MYC-DR and MYC-WT measured in a melanoma cell line (A375) treated with 1.0 μM Corin and representative immunoblots from three biological replicates. **F)** Immunoblots of FLAG-tagged MYC in lenti-X-293T cells with ectopic overexpression of p300 and CBP histone acetyltransferases in relation to empty vector control cells. **G)** Immunoblots of HA-tagged MYC in WM983B cells treated with vehicle control (DMSO), Corin (1.0 μM), HAT inhibitor (HATi) A485 (3.0 μM), and Corin + HATi combination for 24 hrs. Mean with Student's t-test, two-sided, * $p<0.05$. **H)** MYC ubiquitination assay in WM983B cells. N-terminal Flag-tagged MYC-WT and MYC-DR were ectopically expressed followed by ubiquitin assay. MYC was immunoprecipitated by anti-Flag antibody and blotted with anti-ubiquitin antibody. **I)** Quantification of mutant MYC-DR stability in WM983B cells. HA-tagged mutant MYC-DR and wildtype MYC-WT were stably expressed using lentivirus. CHX (10 μM) was added to block cellular protein synthesis at different time points. Representative immunoblots of triplicates (top) and HA-MYC quantification (bottom). The HA-MYC level at each time point is represented relative to the level at time zero. **J)** Kaplan-Meier survival curves of melanoma patient groups with high and low expressions of MYC protein and transcript levels defined by median expression across patients (SKCM TCGA dataset). RPPA (reverse phase protein array) and RNA-seq datasets were used for MYC protein and mRNA expressions, respectively.

Fig. 3. CoREST-complex transcriptionally upregulates genes functionally associated with RNA processing in melanoma. A) Differentially expressed genes (DEGs) in melanoma cells with RCOR1 knockdown (KD) compared to isogenic control cells. **B)** Gene Set Enrichment Analysis (GSEA) showing the top enriched categories for genes differentially expressed by RCOR1 KD in melanoma cells. **C)** Expression heatmap of genes differentially expressed in the RCOR1 KD. Genes were selected from the gene set of mRNA processing (GO:0006367) that are commonly down-regulated in all three melanoma cell lines (WM983B, A375, and SK-MEL2) with RCOR1 KD. Legend indicates fraction of TPM values (control vs. RCOR1 KD). **D)** Analysis of consequences of switching in mRNA processing of RCOR1 KD cells relative to the control cells. The analyzed consequences expressed in fractions are gain or loss of exon, intron retention, isoform length, isoform sequence similarity, complete open reading frame (ORF), ORF length and similarity, nonsense-mediated decay (NMD) sensitivity, and position change of last exon, transcription start, and termination sites. **E)** Validation of exon skipping and retention of exons 2, 6, and 2 of PELO, STX1A, and FAM20C genes, respectively, by semi-quantitative RT-PCR analysis in RCOR1-KD cells relative to the control cells. Quantification of three biological replicates is shown on the left, and a representative example is shown in the right panels. Data are mean with s.d. and Student's t-test (two-sided) was used; *$P<0.05$ and **$P<0.01$.

Fig. 4. CoREST-complex cooperates with MYC to control the transcription of a subset of genes involved in the biological steps of RNA processing in melanoma. A) Venn diagram showing counts of genes occupied by RCOR1 and MYC within the regulatory regions of ±2.0 kbps from the TSS of genes regulated by the proteins in the A375 cell genome. **B)** Base pair distance of RCOR1 and MYC from the TSS in the A375 cell genome and absolute distance between RCOR1- and MYC-binding motifs occupied in the regulatory regions of a gene set involved in RNA processing (GO:00006396). **C)** RCOR1 binding motifs and predicted GO terms

that are specific to the motif binding factor RCOR1 in A375 melanoma cells. **D)** Venn diagram showing counts of genes harboring RCOR1 ChIP-seq peaks and MYC ChIP-seq peaks at the regulatory regions of RNA processing genes. **E)** Re-ChIP PCR analysis at the proximal promoter regions of genes selected from the 62 genes co-regulated by CoREST-complex and MYC. The data indicates fold-change enrichment. **F)** Semi-quantitative RT-PCR assay of selected genes from the gene set of RNA processing (GO:00006396) that are down-regulated in all three melanoma cell lines (A375, SK-MEL2, and WM983B) with RCOR1-KD compared to isogenic control cell lines. **G)** Pearson correlation coefficient (r) with statistical significances (q-value <0.001) between the expression of RCOR1 and each of the 62 genes annotated with RNA processing and co-occupied by both RCOR1 and MYC in the promoter region. Patients with cutaneous melanoma (SKCM) and all other cancer types (Pan-cancer) in TCGA data sets were used. **H)** Kaplan-Meier survival curves of melanoma patient groups with high and low expressions of NOLC1/NOPP140 gene transcript levels defined by median expression across patients (SKCM TCGA dataset). **I)** Relative growth assay of A375 cells with RCOR1-KD, NOLC1-KD, and RCOR1-KD + NOLC1-OE (ectopic overexpression) compared to isogenic control cells. The knockdown (KD) and overexpression (OE) of the respective genes were confirmed by immunoblot (right). Data with SD, t-test (2-sided), ***p<0.001.

Figures:

Figure 1

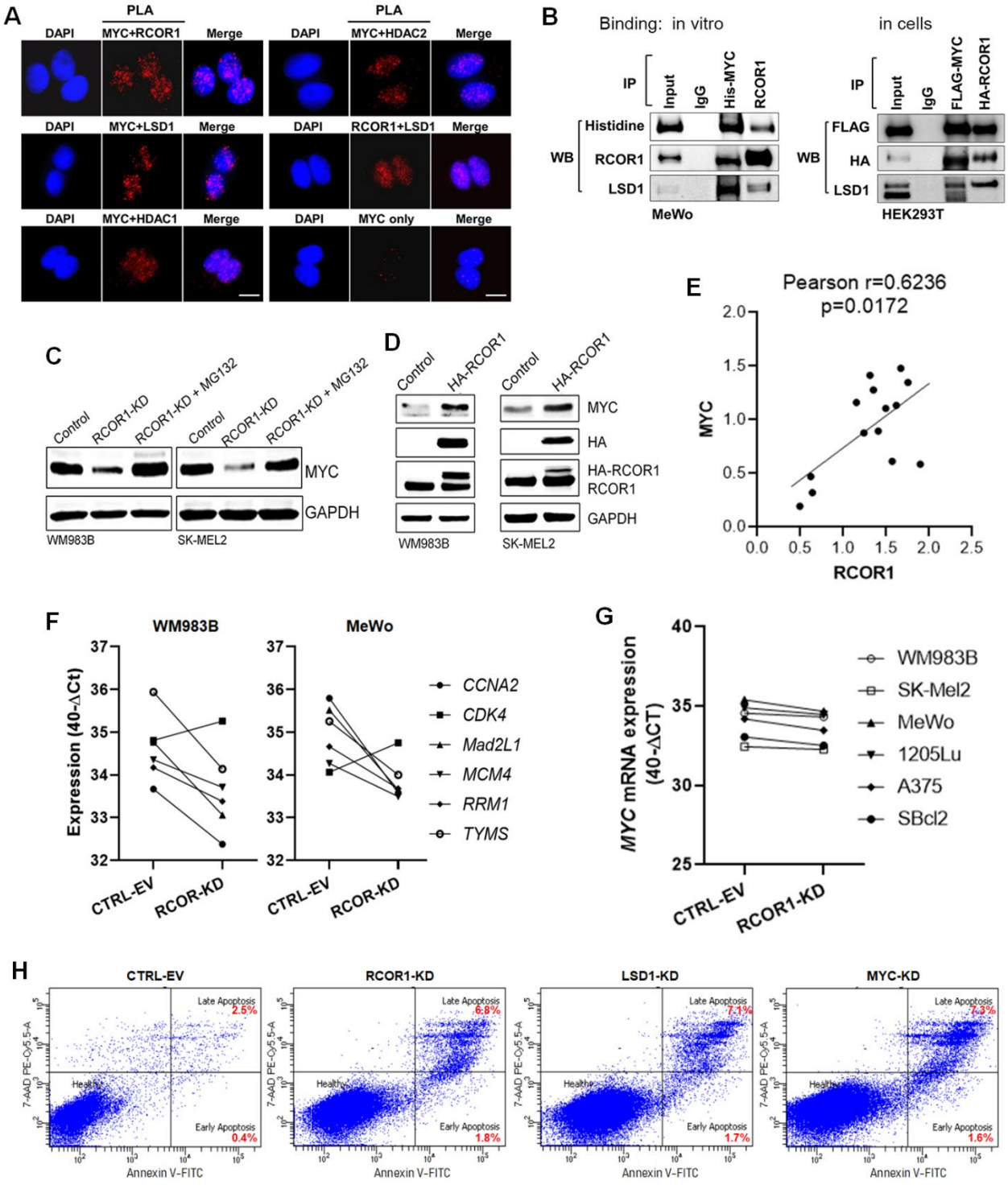

Figure 2

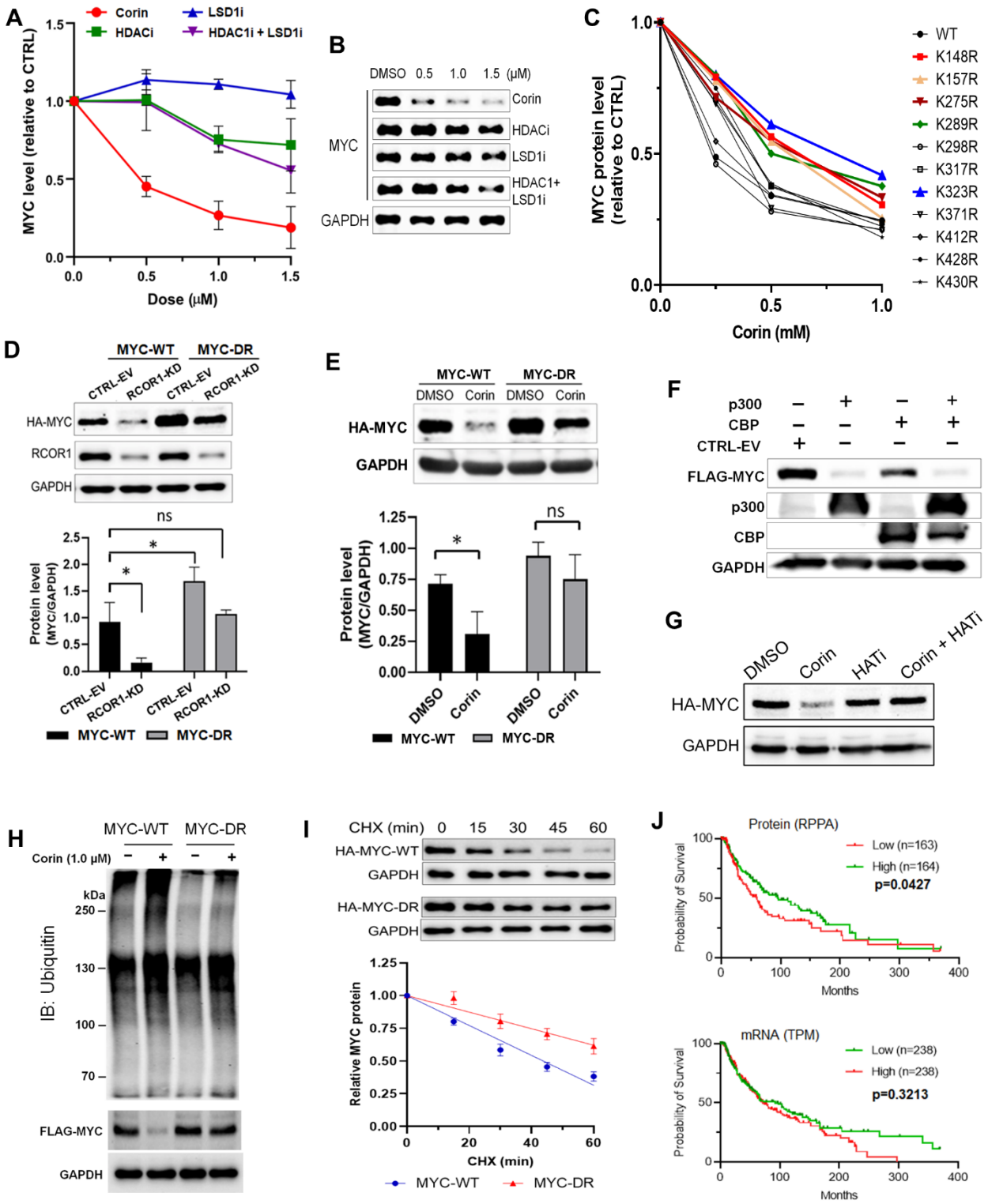
A
Corin
HDACi
LSD1i
HDAC1i + LSD1i
MYC level (relative to CTRL)
Dose (μM)
B
DMSO 0.5 1.0 1.5 (μM)
MYC
Corin
HDACi
LSD1i
HDAC1+ LSD1i
GAPDH
C
MYC protein level (relative to CTRL)
Corin (mM)
WT
K148R
K157R
K275R
K289R
K298R
K317R
K323R
K371R
K412R
K428R
K430R
D
MYC-WT
MYC-DR
CTRL-EV
RCOR1-KD
HA-MYC
RCOR1
GAPDH
Protein level (MYC/GAPDH)
ns
*
E
MYC-WT
MYC-DR
DMSO
Corin
HA-MYC
GAPDH
Protein level (MYC/GAPDH)
F
p300
CBP
CTRL-EV
FLAG-MYC
p300
CBP
GAPDH
G
DMSO
Corin
HATi
Corin + HATi
HA-MYC
GAPDH
H
MYC-WT
MYC-DR
Corin (1.0 μM)
kDa
250
130
100
70
IB: Ubiquitin
FLAG-MYC
GAPDH
I
CHX (min) 0 15 30 45 60
HA-MYC-WT
GAPDH
HA-MYC-DR
GAPDH
Relative MYC protein
CHX (min)
MYC-WT
MYC-DR
J
Protein (RPPA)
Low (n=163)
High (n=164)
p=0.0427
Probability of Survival
Months
mRNA (TPM)
Low (n=238)
High (n=238)
p=0.3213
Probability of Survival
Months

Figure 3

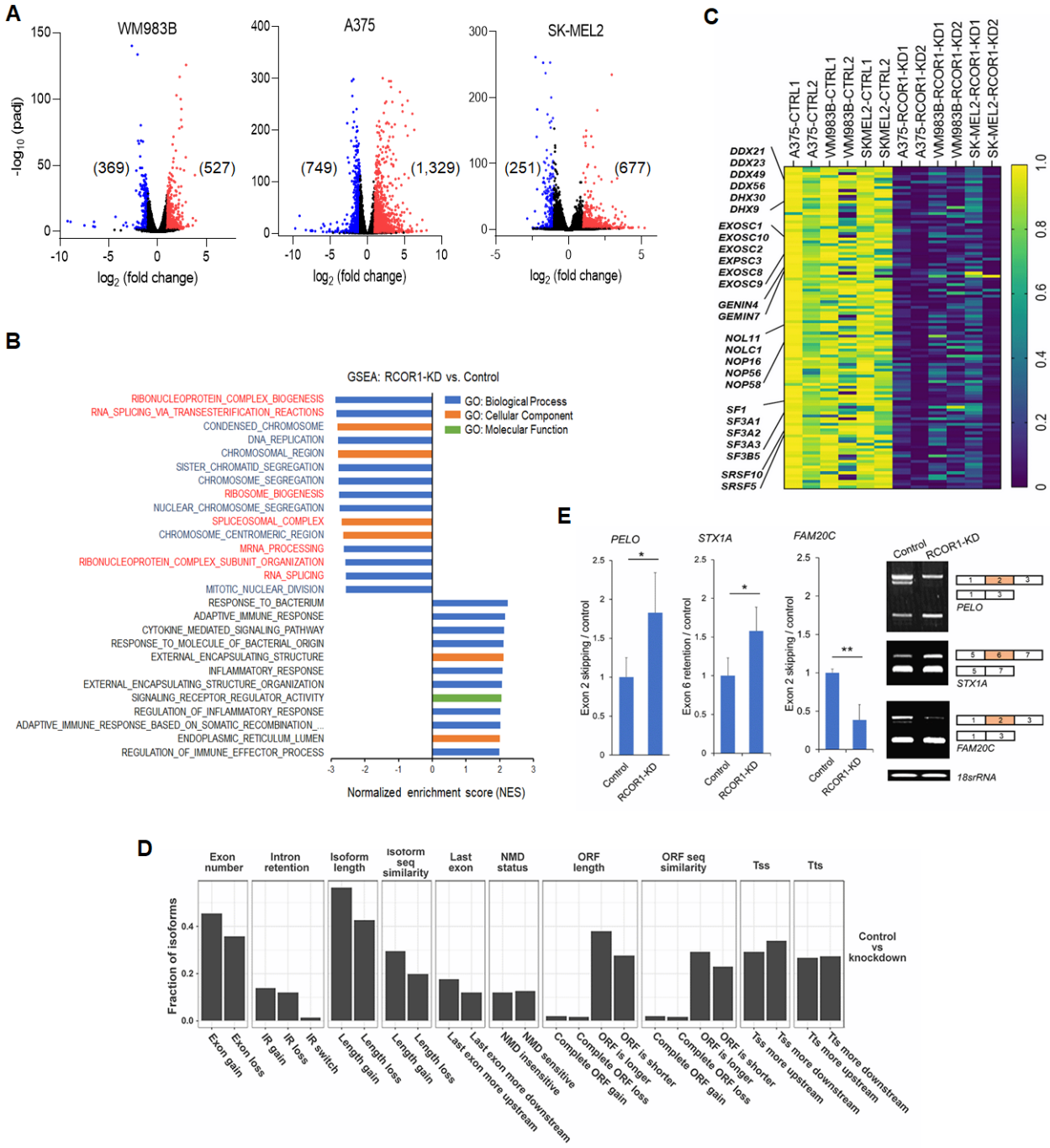
A
WM983B
A375
SK-MEL2
-log10 (padj)
(369)
(527)
(749)
(1,329)
(251)
(677)
log2 (fold change)
B
GSEA: RCOR1-KD vs. Control
GO: Biological Process
GO: Cellular Component
GO: Molecular Function
RIBONUCLEOPROTEIN_COMPLEX_BIOGENESIS
RNA_SPLICING_VIA_TRANSESTERIFICATION_REACTIONS
CONDENSED_CHROMOSOME
DNA_REPLICATION
CHROMOSOMAL_REGION
SISTER_CHROMATID_SEGREGATION
CHROMOSOME_SEGREGATION
RIBOSOME_BIOGENESIS
NUCLEAR_CHROMOSOME_SEGREGATION
SPLICEOSOMAL_COMPLEX
CHROMOSOME_CENTROMERIC_REGION
MRNA_PROCESSING
RIBONUCLEOPROTEIN_COMPLEX_SUBUNIT_ORGANIZATION
RNA_SPLICING
MITOTIC_NUCLEAR_DIVISION
RESPONSE_TO_BACTERIUM
ADAPTIVE_IMMUNE_RESPONSE
CYTOKINE_MEDIATED_SIGNALING_PATHWAY
RESPONSE_TO_MOLECULE_OF_BACTERIAL_ORIGIN
EXTERNAL_ENCAPSULATING_STRUCTURE
INFLAMMATORY_RESPONSE
EXTERNAL_ENCAPSULATING_STRUCTURE_ORGANIZATION
SIGNALING_RECEPTOR_REGULATOR_ACTIVITY
REGULATION_OF_INFLAMMATORY_RESPONSE
ADAPTIVE_IMMUNE_RESPONSE_BASED_ON_SOMATIC_RECOMBINATION_...
ENDOPLASMIC_RETICULUM_LUMEN
REGULATION_OF_IMMUNE_EFFECTOR_PROCESS
Normalized enrichment score (NES)
C
A375-CTRL1
A375-CTRL2
WM983B-CTRL1
WM983B-CTRL2
SKMEL2-CTRL1
SKMEL2-CTRL2
A375-RCOR1-KD1
A375-RCOR1-KD2
WM983B-RCOR1-KD1
WM983B-RCOR1-KD2
SK-MEL2-RCOR1-KD1
SK-MEL2-RCOR1-KD2
DDX21
DDX23
DDX49
DDX56
DHX30
DHX9
EXOSC1
EXOSC10
EXOSC2
EXPSC3
EXOSC8
EXOSC9
GENIN4
GEMIN7
NOL11
NOLC1
NOP16
NOP56
NOP58
SF1
SF3A1
SF3A2
SF3A3
SF3B5
SRSF10
SRSF5
E
PELO
STX1A
FAM20C
Exon 2 skipping / control
Exon 6 retention / control
Control
RCOR1-KD
18srRNA
D
Exon number
Intron retention
Isoform length
Isoform seq similarity
Last exon
NMD status
ORF length
ORF seq similarity
Tss
Tts
Fraction of isoforms
Control vs knockdown
Exon gain
Exon loss
IR gain
IR loss
IR switch
Length gain
Length loss
Last exon more upstream
Last exon more downstream
NMD insensitive
NMD sensitive
Complete ORF gain
Complete ORF loss
ORF is longer
ORF is shorter
Tss more upstream
Tss more downstream
Tts more upstream
Tts more downstream

Figure 4

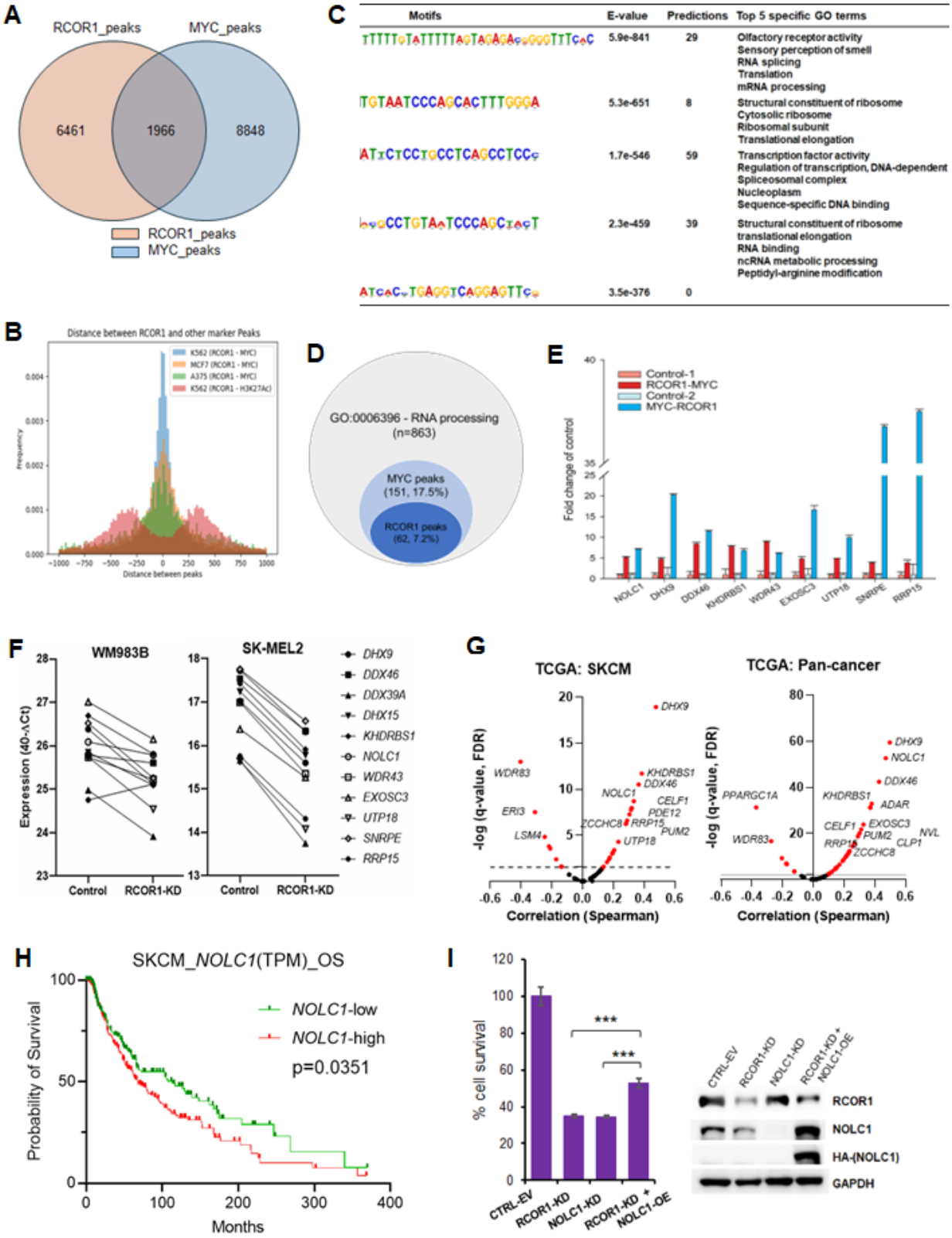
A
RCOR1_peaks
MYC_peaks
6461
1966
8848
RCOR1_peaks
MYC_peaks
C
Motifs
E-value
Predictions
Top 5 specific GO terms
5.9e-841
29
Olfactory receptor activity
Sensory perception of smell
RNA splicing
Translation
mRNA processing
5.3e-651
8
Structural constituent of ribosome
Cytosolic ribosome
Ribosomal subunit
Translational elongation
1.7e-546
59
Transcription factor activity
Regulation of transcription, DNA-dependent
Spliceosomal complex
Nucleoplasm
Sequence-specific DNA binding
2.3e-459
39
Structural constituent of ribosome
translational elongation
RNA binding
ncRNA metabolic processing
Peptidyl-arginine modification
3.5e-376
0
B
Distance between RCOR1 and other marker Peaks
K562 (RCOR1 - MYC)
MCF7 (RCOR1 - MYC)
A375 (RCOR1 - MYC)
K562 (RCOR1 - H3K27Ac)
Frequency
Distance between peaks
D
GO:0006396 - RNA processing
(n=863)
MYC peaks
(151, 17.5%)
RCOR1 peaks
(62, 7.2%)
E
Control-1
RCOR1-MYC
Control-2
MYC-RCOR1
Fold change of control
NOLC1
DHX9
DDX46
KHDRBS1
WDR43
EXOSC3
UTP18
SNRPE
RRP15
F
WM983B
SK-MEL2
Expression (40-ΔCt)
Control
RCOR1-KD
DHX9
DDX46
DDX39A
DHX15
KHDRBS1
NOLC1
WDR43
EXOSC3
UTP18
SNRPE
RRP15
G
TCGA: SKCM
TCGA: Pan-cancer
-log (q-value, FDR)
Correlation (Spearman)
DHX9
NOLC1
DDX46
KHDRBS1
ADAR
EXOSC3
PUM2
CLP1
NVL
ZCCHC8
RRP15
CELF1
WDR83
PPARGC1A
ERI3
LSM4
PDE12
H
SKCM_NOLC1(TPM)_OS
NOLC1-low
NOLC1-high
p=0.0351
Probability of Survival
Months
I
% cell survival
CTRL-EV
RCOR1-KD
NOLC1-KD
RCOR1-KD + NOLC1-OE
RCOR1
NOLC1
HA-(NOLC1)
GAPDH